Geochemical Perspectives Letters

© 2023 The Authors
Published by the European Association of Geochemistry

Bacterial use of siderophores increases olivine dissolution rates by nearly an order of magnitude

A. Lunstrum, M. Van Den Berghe, X. Bian, S. John, K.H. Nealson, A.J. West

Supplementary Information

The Supplementary Information includes:

- Methods
- Results
- Table S-1
- Figures S-1 to S-5
- Supplementary Information References

Methods

The experiment consisted of batch reactors containing olivine grains, Fe-deplete growth medium, and the following treatments: wild type *Shewanella oneidensis* (MR-1); a gene-deletion mutant of MR-1 incapable of producing siderophores (ΔMR-1); ΔMR-1 with added deferoxamine B (ΔMR-1 + DFOB, ranging from 0 to 50 µM); ΔMR-1 killed control; and abiotic treatments with no microbes but added DFOB (ranging from 0 to 50 µM). All treatments, listed in Table S-1, were conducted in triplicate. Henceforth, the live MR-1 and ΔMR-1 treatments are collectively referred to as "biotic", whereas the solutions with no microbial addition are referred to as "abiotic". Note that ΔMR-1 (*i.e.* ΔSO3031) was previously characterised as being incapable of producing siderophores but capable of utilising them through the hydroxamate reductase pathway (Fennessey *et al*., 2010). Furthermore, MR-1 is capable of taking up a range of siderophores, including the tris-hydroxamate DFOB, in addition to its native di-hydroxamate siderophore, putrebactin (Liu *et al*., 2018; Van Den Berghe *et al*., 2021).

Materials preparation. Olivine grains were collected from the University of Southern California mineral collection and were hand-crushed with a clean mortar and pestle. Crushed material was sieved to 150–300 µm diameter, ultrasonicated and rinsed seven times (5 min sonication *per* rinse) in 200-proof ethanol, then air-dried in an oven at 130 °C overnight. Immediately before the experiments, olivine grains were UV-sterilised for 30 min. Elemental composition of the olivine was analysed by X-ray fluorescence (XRF; Bruker S8 Tiger). By assuming a spherical shape and binning into six grain sizes with a normal distribution, the grain size distribution yielded a mean mineral surface area of 10,640 $mm^2\ g^{-1}$.

All experiments and sample analyses were performed in a laminar flow hood to prevent microbial and/or metal contamination. Furthermore, experiments and all media preparation were performed in acid-washed polycarbonate or polypropylene containers to avoid potential metal contamination from biotically induced glass dissolution (Gorbushina and Palinska, 1999; Aouad *et al*., 2006). The pH 7.2 growth medium was based on the M-1 minimal medium (Gorby *et al*., 2006), slightly modified by using MOPS buffer (50 mM) and N-acetyl glucosamine (18 mM) as the carbon source

and electron donor, in place of carboxylic acids that are known to enhance mineral dissolution abiotically (Neaman *et al*., 2005; Olsen and Rimstidt, 2008). Furthermore, Fe was omitted from the growth medium so that olivine was the only available Fe source. A detailed description of the growth medium composition is provided in Van Den Berghe *et al*. (2021). pH was confirmed at the beginning of the experiment and, given the high buffering capacity and relatively short duration of the experiment, was assumed to not change significantly over the course of the experiment.

For the biotic experiments, inoculation cultures were grown from individual isolated colonies and conditioned prior to the experiments in the same minimal medium (though Fe-replete, with 3.6 μM $FeSO_4$), without olivine. Microbes were extracted from these growth solutions by filtering (<0.2 μm), then triple-rinsed and concentrated in Fe-free medium prior to inoculation.

Batch reactor experiments. Batch reactor experiments were performed in Erlenmeyer flasks exposed to atmospheric conditions *via* porous caps, maintained in the dark at 30 °C, and shaken continuously at 120 rpm. 100 mL of the Fe-deplete medium was added to each flask, followed by inoculation cultures (for biotic experiments), and siderophore solution (for DFOB addition experiments). 100 mg olivine was then added to each flask. Flasks for the killed ΔMR-1 control treatment were autoclaved after inoculation, but prior to adding olivine.

For all biotic experiments, flasks were inoculated with approximately 5×10^{10} cells (for a starting cell concentration of approximately 5×10^{8} cells mL^{-1}). This initial cell density was selected to rapidly achieve maximum cell concentration. At each sampling time, 1 mL samples were extracted to monitor growth by optical density (OD) measurements, using pre-determined OD *vs*. cell count relationships (600 nm wavelength on Shimadzu UV-2600 spectrophotometer). Additional information on cell count methods is presented in Van Den Berghe *et al*. (2021).

For the ΔMR-1 + DFOB and abiotic DFOB treatments, a filter-sterilised stock solution of deferoxamine mesylate (Sigma Aldrich, US) was added to reach final concentrations ranging from 0.05 to 50 μM (Table S-1). A maximum of 50 μM was used based on prior findings that >5 μM DFOB addition was sufficient to stimulate maximum ΔMR-1 growth (Van Den Berghe *et al*., 2021). While DFOB is a tris-hydroxamate, structurally different from the cyclic di-hydroxamate putrebactin, it is known to be readily bioavailable to ΔMR-1.

Most experiments were run for approximately 48 h, just long enough for the biotic treatments to complete exponential growth and maintain stationary phase for ≥12 hours. A subset of experiments was run for 79 h to assess dissolution rates over a longer time period. Over the course of the experiments, samples were extracted (without volume replacement) for elemental analyses, ensuring homogenous sampling of suspended material by gently swirling bottles.

Elemental analysis of experimental solution. For experiments marked "OES" in Table S-1, dissolved Si was measured by inductively coupled plasma optical emission spectrometry (ICP-OES, Agilent 5100) at emission wavelengths of 251.611 nm. Because dissolved metal measurements in these experiments were either below ICP-OES detection (for Fe) or lower than the medium initial values (for Mg), we ran additional experiments for analysis of dissolved and solid phase metals by inductively coupled plasma mass spectrometry (ICP-MS, Thermofisher Scientific Element2); these are marked "ICP-MS, OES" in Table S-1.

For the OES only experiments, ~5 mL samples were taken at each timepoint, then filtered, acidified to ~0.5 % HNO_3, and preserved in the dark at 4 °C until analysis. Because Si does not have any biological function in *Shewanella* and is not a component of the minimal medium, dissolved Si was assumed to represent total dissolution flux from the mineral. For the ICP-MS, OES experiments, ~5 mL samples were taken at each timepoint, and separated into unfiltered and filtered (0.2 μm) aliquots. All samples were then acidified to 2 % HNO_3 and stored in the dark at room temperature until analysis. Prior to analysis, 100 μL aliquots were digested to prevent analytical interference by the organic matrix. Aliquots were added to PFA vials, acidified with 1 mL each of concentrated HCl and HNO_3, and dried at 120 °C overnight. Subsequently, dried samples were digested once more by adding 1 mL concentrated HNO_3, heating at 120 °C for 2–3 h, then drying at 120 °C overnight. Finally, samples were reconstituted with 1 mL 0.1 N HNO_3, with the addition of 10 ppb indium (In) as the internal standard to monitor analytical drift and correct for matrix effects. This multiple digestion procedure ensures the destruction of organic compounds and the complete dissolution of all available Fe. Measurements were taken for all metals present in the mineral (Table S-1). This digestion procedure resulted in significant Si loss, so additional aliquots of undigested, filtered samples were analysed for Si on the OES. For the OES analysis, 0.5 to 1 mL aliquots were reconstituted to 2.5 mL with Si-free growth medium, acidified to 2 % HNO_3, then analysed on the OES as described above.

Data analysis. All data analysis was performed in Python v 3.8.8.

Erroneous measurements were removed from the dataset *via* an automated quality control procedure based on replicate standard deviation, and/or obvious erroneous points (*e.g.*, unrealistically high or negative values) removed manually. Specifically, outliers were removed when triplicate standard deviation exceeded 50 % of the triplicate mean. This resulted, in for example, four Si data removed (out of 365), and 33 Fe data removed (out of 328). The higher rate of erroneous data with Fe is due to lower concentrations near analytical detection limits as well as higher probability of contamination during sample processing. Measured Si and metal concentrations at each timepoint (C_i) were corrected ($C_{i,\ \text{correct}}$) to consider mass extracted at prior timepoints: $C_{i,\text{correct}} = (C_i V_i + \sum_{j=1}^{(i-1)} v\, C_j)/V_0$ where V_i is the experimental volume remaining prior to sampling time i, v is the sample volume, C_j is the measured concentration at each prior timepoint, and V_0 is the initial experimental volume (100 mL).

Dissolution rates were inferred from changes in Si concentrations as Si, unlike Mg or Fe, is not used by *Shewanella* and is not a component of the minimal medium. Furthermore, Mg is highly exchangeable with protons at the initiation of dissolution experiments, and Fe easily precipitates as insoluble Fe-oxide secondary minerals, making both metals potentially misleading for calculation of net dissolution rate (Reichard *et al*., 2007; Oelkers *et al*., 2018). Dissolution rates were calculated based on the slope of corrected Si concentration *vs*. time ($\Delta Si/\Delta t$), considering only timepoints between 23 and 53 h, so as to exclude early timepoints with little microbial activity and later timepoints with significant accumulation of dead cells. This window captured the transition from exponential growth to stationary phase (Fig. S-2). These rates were normalised by either mineral mass (g^{-1}) or mineral surface area (m^{-2}). Rates were calculated for each bottle individually, then replicate bottles for the same treatment were averaged to yield a single dissolution value for each treatment. The dissolution rate for each treatment was considered statistically significant (*i.e.* significantly different from a rate of 0) if at least two of the three replicate bottles had p values <0.05.

Results

Olivine elemental composition. The cation composition of the ground olivine was 87.1 % Mg, 11.9 % Fe, and 0.5 % each of Ca and Ni, with trace amounts of Mn, Cr, Co, Zn, and Cu (Table S-1). The overall chemical composition is summarised as $Mg_{1.76}Fe_{0.24}SiO_4$ (*i.e.* Fo_{88}; predominantly forsterite with approximately 12 % Fe-containing fayalite in the solid solution).

Growth curves. Experiments with MR-1 and ΔMR-1 with added DFOB of at least 0.2 µM all exhibited exponential cell growth, reaching stationary phase between 24 to 40 h (Fig. S-1). Growth of the mutant ΔMR-1 scaled with DFOB addition, with no growth at DFOB < 0.2 µM, significant but inhibited growth with added DFOB between 0.2 and 1 µM, and maximum growth reached at 50 µM DFOB addition. Previous research using identical methods showed that cell density for ΔMR-1 maximises at approximately 5 µM DFOB addition, so ΔMR-1 + DFOB (50 µM) was not siderophore-limited (Van Den Berghe *et al*., 2021). Wild type MR-1 stationary cell density (8×10^9 cells mL^{-1}) was nearly double that of the ΔMR-1 + DFOB (50 µM) treatment (4×10^9 cells mL^{-1}).

Silicon and metal cation release rates. Dissolved Si was measurable in all samples, but the release rate during the stationary phase window considered was only significant for some treatments (Fig. 1a, b; Table S-1). In the abiotic treatments, Si release scaled with DFOB concentration, ranging from 0.02 to 0.04 µmol g^{-1} h^{-1}, and was significant for all DFOB additions, including the lowest concentration of 0.05 µM DFOB. In contrast, Si release in the ΔMR-1 + DFOB treatments was more variable and was not significant (at level of OES analytical detection) until at least 1 µM DFOB addition. Once detectable, Si release rates in the biotic treatments were higher than in the abiotic treatments at the same DFOB concentration, reaching 0.27 µmol g^{-1} h^{-1} in the ΔMR-1 + DFOB (50 µM) treatment. Si release in wild type MR-1 was comparably high, reaching 0.25 µmol g^{-1} h^{-1}. The change in Si release rate over time also varied between biotic and abiotic experiments. In abiotic conditions, Si release was fastest between 0 and 24 hours, followed by relatively slower rates, similar to other abiotic experiments with siderophores (Torres *et al*., 2019). In contrast, the biotic experiments typically had relatively constant release rates during the measurement period, and if anything, slower initial rates. However, wild type MR-1 uniquely exhibited a slowing of Si release rates shortly after reaching stationary phase, after approximately 40 h.

Total Fe release closely mirrored Si, with increasing Fe in all biotic treatments with siderophore addition (Fig. 1c). For the time period considered (23–53 h), however, release rates were only significant in the MR-1 and ΔMR-1 + DFOB (50 μM) treatments. Considering the later timepoint, ΔMR-1 + DFOB (0.2 μM) also had a significant Fe release rate. The ΔMR-1 + DFOB (50 μM) treatment showed a consistent release rate of 0.05 μmol g^{-1} h^{-1}, whereas the release rate for MR-1 wild type was initially similar, but slowed after stationary phase was achieved at 40 h. Prior to 40 h, there was no significant dissolved Fe in any treatment, implying the total Fe increase was entirely shunted to biomass. (In this study, we assume particulate Fe and Mg to be in biomass. While it is possible that metals may adsorb to cell exteriors, a distinction between internal or adsorbed Fe does not affect our analysis.) In the MR-1 treatment, dissolved Fe remained near zero for the duration for the experiment. However, in all ΔMR-1 treatments, dissolved Fe increased after 40 h, following the total Fe trend, implying accumulation of Fe in dissolved phase but no change in the particulate Fe pool.

In contrast to Si, total Mg was initially stable or decreased slightly, followed by an increase after approximately 24 h (Fig. S-3). Only the ΔMR-1 + DFOB (50 μM) treatment showed sustained Mg release through the end of the experiment, whereas Mg concentrations in the other treatments stabilised after about 40 h. Replicate variability for these latter timepoints was relatively high, however, precluding clear trends. Considering dissolved Mg, both biotic treatments with high growth rates (MR-1 and MR-1Δ + DFOB (50 μM)) showed a significant reduction in dissolved Mg during the exponential growth phase, with an increase in dissolved Mg thereafter.

Compared to the known mineral stoichiometry, elemental ratios of Si, Mg, and Fe showed disproportionate Si release for the first ~30 h of the experiment (Fig. S-4a, b). After 40 h, Mg release increased for all treatments and Mg/Si appeared to remain congruent for the duration of the experiment, although sample error was high. Total Fe followed a similar pattern for the ΔMR-1 treatments, with congruent Fe/Si after approximately 30 h. For the MR-1 and control treatments, however, Fe/Si remained depressed at about 60 % of expected stoichiometry.

For trace metals, only Ni exhibited any significant release, and then only for the ΔMR-1 + DFOB (50 μM) treatment, with a release rate of 0.004 ± 0.001 μmol Ni g olivine^{-1} h^{-1} (Fig. S-5). Dissolved and total Ni concentrations were similar, implying that Ni was not taken up by, or adsorbed to, biomass. All other metals showed no trends over time that exceeded analytical uncertainty.

Supplementary Table

Table S-1 Experimental details and elemental release rates for Si and Fe (mean ± s.d.). '--', not measured; *n.s.*, not significantly different from 0.

Category	Treatment	DFOB (µM)	Experiment Length (h)	Analysis	Si release (µmol g^{-1} h^{-1})	Fe release (µmol g^{-1} h^{-1})
Biotic	MR-1	0	79	ICP-MS, OES	0.23 ± 0.01	0.04 ± 0.01
	MR-1	0	46	OES	0.25 ± 0.02	--
	ΔMR-1	0	79	ICP-MS, OES	*n.s.*	*n.s.*
	ΔMR-1	0	53	OES	*n.s.*	--
	ΔMR-1 + DFOB	0.05	53	OES	*n.s.*	--
	ΔMR-1 + DFOB	0.2	79	ICP-MS, OES	*n.s.*	*n.s.*
	ΔMR-1 + DFOB	1	53	OES	0.06 ± 0.01	--
	ΔMR-1 + DFOB	50	79	ICP-MS, OES	0.23 ± 0.01	0.05 ± 0.01
	ΔMR-1 + DFOB	50	46	OES	0.27 ± 0.01	--
Abiotic	Killed ΔMR-1	0	79	ICP-MS, OES	*n.s.*	*n.s.*
	Killed ΔMR-1	0	46	OES	*n.s.*	--
	Control	0	48	OES	*n.s.*	--
	DFOB	0.05	48	OES	0.02 ± 0.01	--
	DFOB	1	48	OES	0.02 ± 0.01	--
	DFOB	50	48	OES	0.04 ± 0.01	--

Supplementary Figures

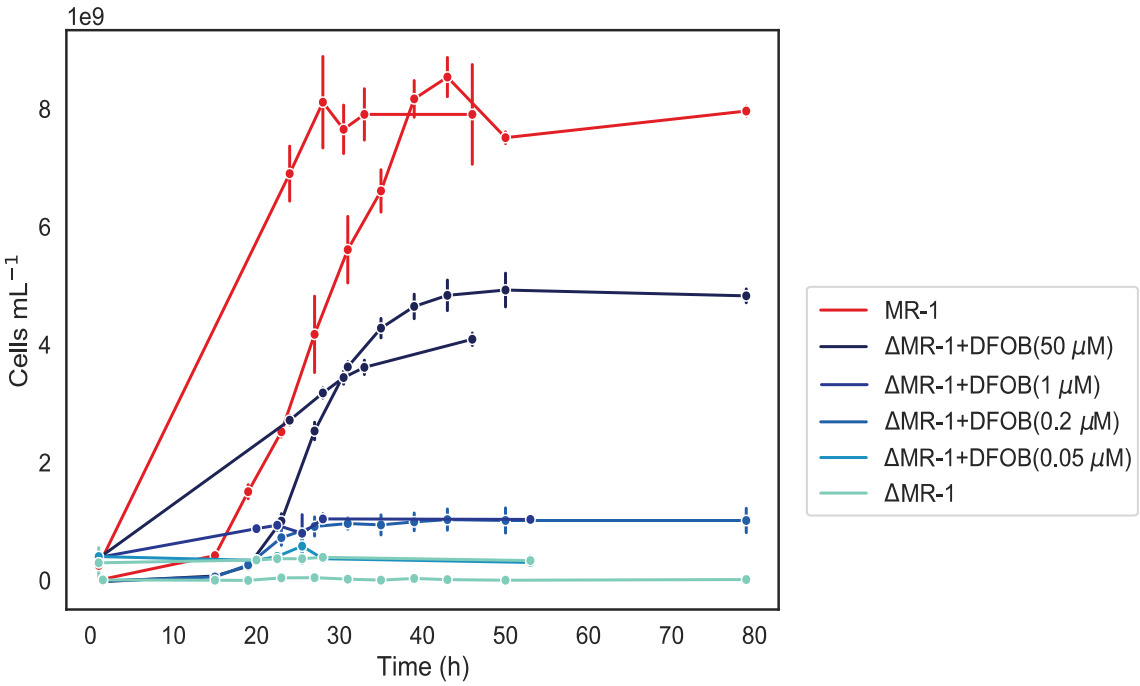

Figure S-1 Growth curves for all biotic treatments. For ΔMR-1 treatments, darker blue shades indicate increasing DFOB addition. All experiments performed in triplicate (error bars are standard deviation). The MR-1 and ΔMR-1 + DFOB (50 μM) experiments were conducted twice; each experimental batch is shown as a separate line in the figure.

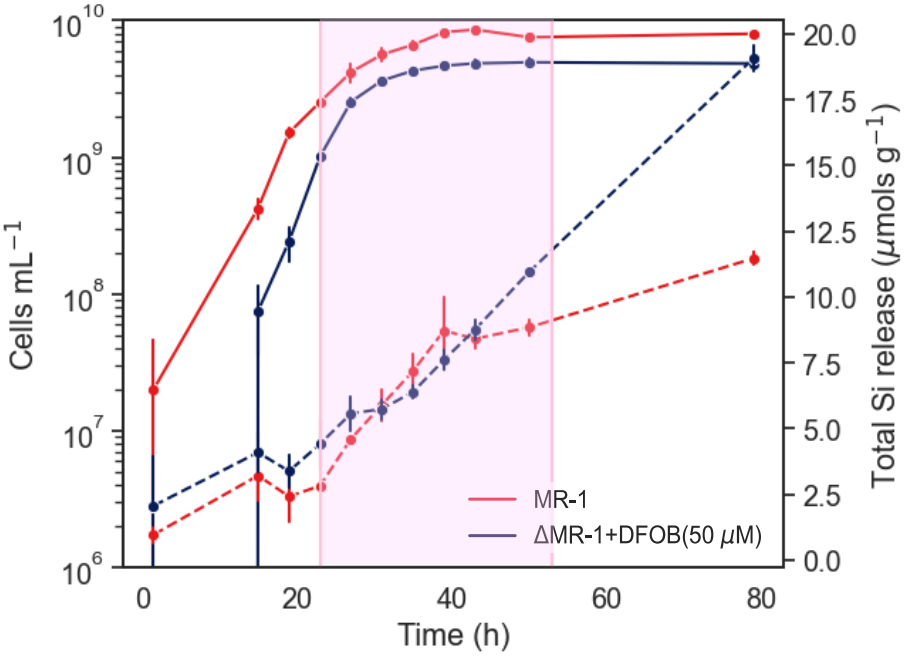

Figure S-2 Examples of growth curves (solid lines, with log-*y* axis) and total Si release (dashed lines) for MR-1 and ΔMR-1 + DFOB (50 µM) experiments. The time-period used to calculate dissolution rates (23 to 53 h) isolates the onset of stationary phase, as highlighted in pink.

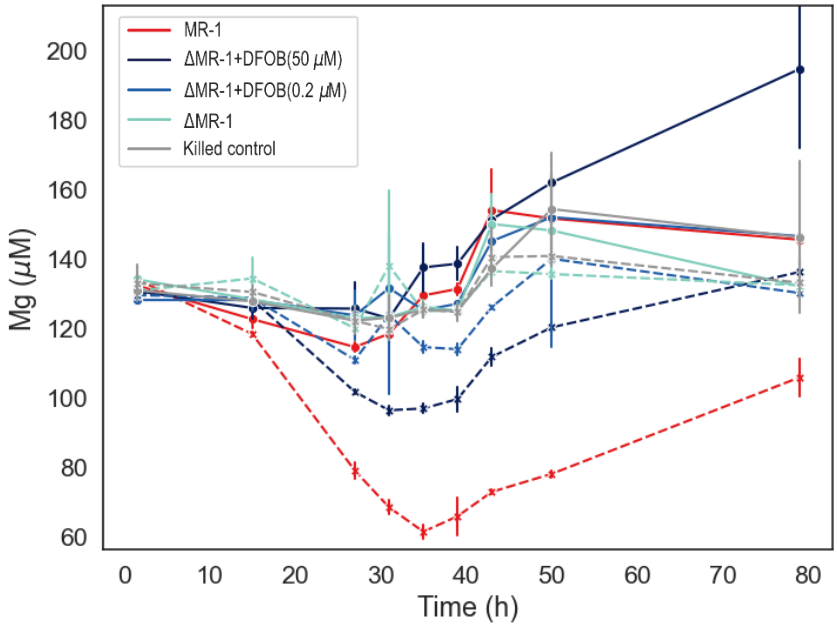

Figure S-3 Dissolved and total Mg *versus* time for the subset of experiments analysed by ICP-MS (mean ± s.d.). Solid lines represent total (unfiltered) elemental release, and dashed lines represent the dissolved (filtered) component.

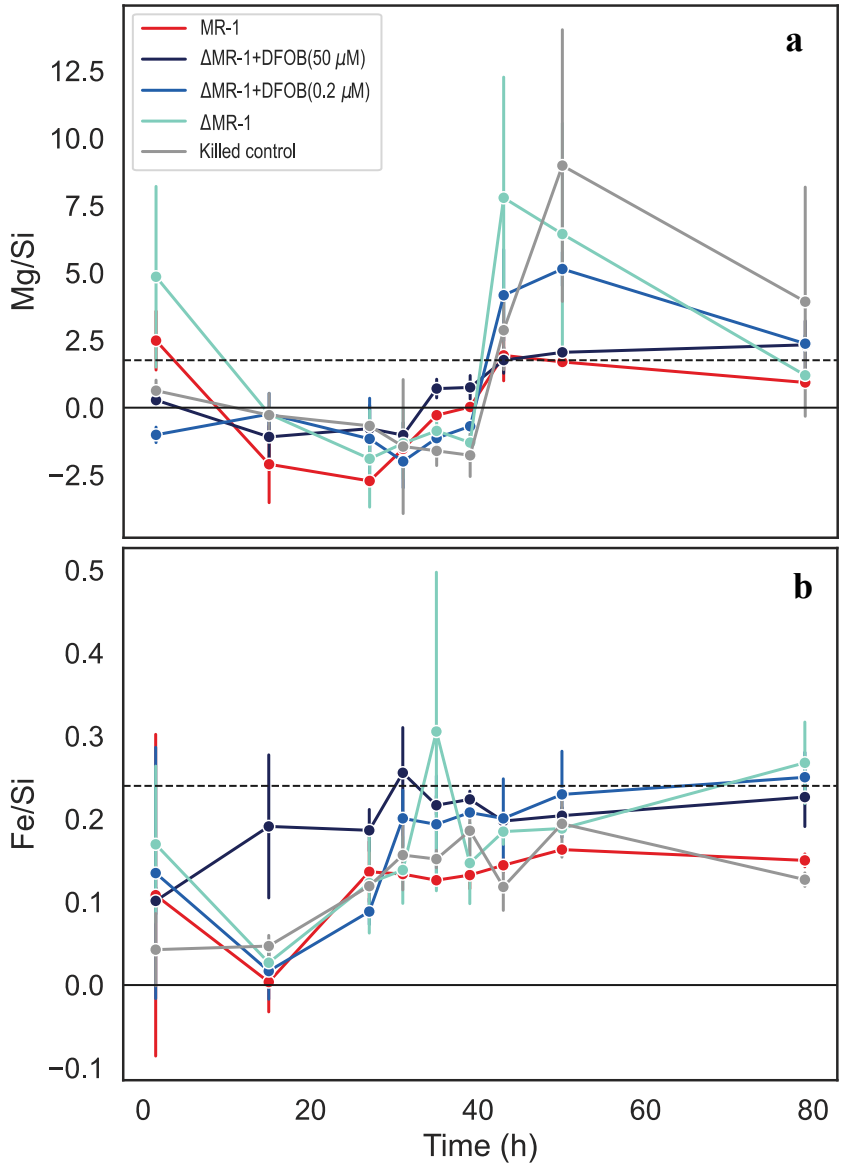

Figure S-4 Elemental ratios of **(a)** total Mg to dissolved Si release and **(b)** total Fe to dissolved Si release *versus* time. Dissolved Si is assumed equivalent to total Si. Dashed lines represent stoichiometry of the source olivine. All experiments performed in triplicate (error bars are standard deviation).

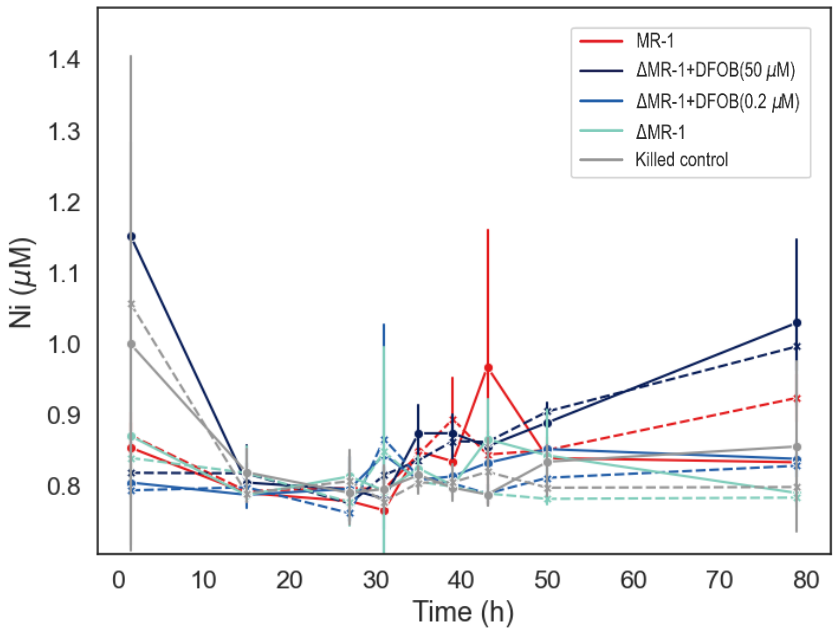

Figure S-5 Dissolved and total Ni *versus* time for the subset of experiments analysed by ICP-MS (mean ± s.d.). Solid lines represent total (unfiltered) elemental release, and dashed lines represent the dissolved (filtered) component. Only the ΔMR-1 + DFOB (50 μM) had a statistically significant Ni release rate.

Supplementary Information References

Aouad, G., Crovisier, J.-L., Geoffroy, V.A., Meyer, J.-M., Stille, P. (2006) Microbially-mediated glass dissolution and sorption of metals by *Pseudomonas aeruginosa* cells and biofilm. *Journal of Hazardous Materials* 136, 889–895. https://doi.org/10.1016/j.jhazmat.2006.01.026

Fennessey, C.M., Jones, M.E., Taillefert, M., DiChristina, T.J. (2010) Siderophores Are Not Involved in Fe(III) Solubilization during Anaerobic Fe(III) Respiration by *Shewanella oneidensis* MR-1. *Applied and Environmental Microbiology* 76, 2425–2432. https://doi.org/10.1128/AEM.03066-09

Gorbushina, A.A., Palinska, K.A. (1999) Biodeteriorative processes on glass: experimental proof of the role of fungi and cyanobacteria. *Aerobiologia* 15, 183–192. https://doi.org/10.1023/A:1007616614172

Gorby, Y.A., Yanina, S., McLean, J.S., Rosso, K.M., Moyles, D., *et al*. (2006) Electrically conductive bacterial nanowires produced by *Shewanella oneidensis* strain MR-1 and other microorganisms. *Proceedings of the National Academy of Sciences* 103, 11358–11363. https://doi.org/10.1073/pnas.0604517103

Liu, L., Li, S., Wang, S., Dong, Z., Gao, H. (2018) Complex Iron Uptake by the Putrebactin-Mediated and Feo Systems in *Shewanella oneidensis*. *Applied and Environmental Microbiology* 84, e01752-18. https://doi.org/10.1128/AEM.01752-18

Neaman, A., Chorover, J., Brantley, S.L. (2005) Implications of the Evolution of Organic Acid Moieties for Basalt Weathering Over Geological Time. *American Journal of Science* 305, 147–185. https://doi.org/10.2475/ajs.305.2.147

Oelkers, E.H., Declercq, J., Saldi, G.D., Gislason, S.R., Schott, J. (2018) Olivine dissolution rates: A critical review. *Chemical Geology* 500, 1–19. https://doi.org/10.1016/j.chemgeo.2018.10.008

Olsen, A.A., Rimstidt, J.D. (2008) Oxalate-promoted forsterite dissolution at low pH. *Geochimica et Cosmochimica Acta* 72, 1758–1766. https://doi.org/10.1016/j.gca.2007.12.026

Reichard, P.U., Kretzschmar, R., Kraemer, S.M. (2007) Dissolution mechanisms of goethite in the presence of siderophores and organic acids. *Geochimica et Cosmochimica Acta* 71, 5635–5650. https://doi.org/10.1016/j.gca.2006.12.022

Torres, M.A., Dong, S., Nealson, K.H., West, A.J. (2019) The kinetics of siderophore-mediated olivine dissolution. *Geobiology* 17, 401–416. https://doi.org/10.1111/gbi.12332

Van Den Berghe, M., Merino, N., Nealson, K.H., West, A.J. (2021) Silicate minerals as a direct source of limiting nutrients: Siderophore synthesis and uptake promote ferric iron bioavailability from olivine and microbial growth. *Geobiology* 19, 618–630. https://doi.org/10.1111/gbi.12457